Green synthesis of Silver and Gold Nanoparticles for Enhanced catalytic and bactericidal activity

IOP Conf. Series: Materials Science and Engineering **263** (2017) 022009 doi:10.1088/1757-899X/263/2/022009

Green synthesis of Silver and Gold Nanoparticles for Enhanced catalytic and bactericidal activity

S Naraginti, N Tiwari and A Sivakumar*
Chemistry Division, School of Advanced Sciences, VIT University, Vellore – 632 014, India

E-mail : svkmr7627@gmail.com

Abstract. A rapid one step green synthetic method using kiwi fruit extract was employed for preparation of silver and gold nanoparticles. The synthesized nanoparticles were successfully used as green catalysts for the reduction of 4-nitrophenol (4-NP) and methylene blue (MB). They also exhibited excellent antimicrobial activity against clinically isolated *Pseudomonas aeruginosa (P.aeruginosa)* and *Staphylococcus aureus (S.aureus)*. It was noticed that with increase in concentration of the aqueous silver and gold solutions, particle size of the Ag and Au NPS showed increase as evidenced from UV-Visible spectroscopy and TEM micrograph. The method employed for the synthesis required only a few minutes for more than 90% formation of nanoparticles when the temperature was raised to 80^{o} C. It was also noticed that the catalytic activity of nanoparticles depends upon the size of the particles. These nanoparticles were observed to be crystalline from the clear lattice fringes in the transmission electron microscopic (TEM) images, bright circular spots in the selected area electron diffraction (SAED) pattern and peaks in the X-ray diffraction (XRD) pattern. The Fourier-transform infrared (FTIR) spectrum indicated the presence of different functional groups in the biomolecule capping the nanoparticles.

1. Introduction

Nanoparticles are known to exhibit characteristic features depending on their size, morphology [1] and these features make them good antibacterial and antifungal agents [2–5]. It is expected that these distinctive properties of nanoparticles would have a vital role in biomedicine, catalysis, optics, energy research and health care [6]. Approaches such as chemical reduction [7], electrochemical reduction [8], photochemical reduction [9] and heat evaporation [10] are all well known. All these methods results into successful production of metal nanoparticles but have disadvantages like high process cost, usage of toxic organic solvents and reducing agents which leads to serious environmental pollution issues. To avoid these issues, green chemistry approaches have been employed for their production [11–15] which are simple, expedient, less energy-exhaustive, ecologically aware and minimize the usage of unsafe materials and maximize the efficiency of the process.
4-nitrophenol (4-NP), listed as a major pollutant by the US EPA [16], is a lavishly used raw material for the production of pesticides, herbicides, synthetic dyes, pharmaceuticals, for processing of leather and in differernt military applications [17]. Since the nitro group in nitrophenols is comparatively static in

biological systems, it could cause health hazards in humans and animals, making it necessary to develop efficient methods for its degradation in environmental samples. This would pave way for degrading hazardous phenolic compounds in water wastes, soil and air which are primary causes of serious health issues in human beings [18, 19]. MB is a thiazine dye, used for trace levels analysis of sulphide ions in aquatic models. MB, in its cationic form finds usage as an anti-malarial and chemotherapeutic agent in aqua culture. It is also used in microbiology, surgery and diagnostics [20,21].
4-nitrophenol and methylene blue have been degraded using different physical and chemical methods employing adsorption, photocatalysis, UV irradiation, microwave, electro catalysis, and fenton reaction, which are energy consuming and require organic solvents. Biological methods have also shown poor degradation on 4-nitrophenol reduction [22, 23]. This made researchers to discover green catalysts for degradation of 4-nitrophenol and methylene, though few reports are available for green catalysis [24, 25], it would be appropriate to develop more efficient and cost-effective methodology for their degradation through an eco-friendly approach. In our previous paper we have also investigated potential bactericidal and catalytic activity of silver nanoparticles using plant extract by green synthesis method [26]. Few reports are also available for bactericidal activity of silver, gold and other metal nanoparticles produced using different plant extracts [27–33].
The present study reports a novel attempt of synthesizing gold and silver nanoparticles using kiwi fruit extract for catalytic reduction of two organic pollutants. Effect of different reactions conditions such as temperature and volume of fruit extract on the formation of nanoparticles were also analyzed. Simultaneously, the bactericidal activity of the synthesized nanoparticles was investigated against clinically isolated pathogenic microorganisms.

2. Materials and methods

2. 1. Chemicals

Silver nitrate ($AgNO_3$) and Chloroauric acid ($HAuCl_4$) were acquired from Sigma-Aldrich chemicals and kiwi fruits were procured from local market. Millipore water was used in all experiments.

2.2. Bacterial pathogens

Clinically isolated bacterial strains *P.aeruginosa* and *S.aureus* from patient blood samples have been obtained from Santhiram Medical College & General Hospital, Nandyal, India.

2.3. fruit extract preparation

Kiwi fruit extract was prepared by taking 100 g of the peeled fruit which was ground well, filtered through Whatmann filter paper and centrifuged at 4000 rpm for 10 min. and stored at 4° C till use.

2.4. Green synthesis of Ag and Au NPs

9 mL of silver nitrate or chloroauric acid (1×10^{-3}M) was mixed with 1 mL of fruit extract and the reaction mixture was placed at 80^{o}C till the color turned to characteristic yellow and ruby-red respectively representing the formation of AgNPs and AuNPs. Both the reactions were carried out at five different concentrations in the range of 1×10^{-3} M to 3×10^{-3} M each of silver nitrate (S_1 to S_5) and chloroauric acid (G_1 to G_5) solutions. These reactions were also carried out at two other temperatures, 30^{o} and 60^{o}C to study rate of the formation of the Ag and Au NPS.

2.5. Characterization of nanoparticles

The effect of fruit extract as reducing agent for the formation of AgNPs and AuPs checked by intermittently measuring the absorbance of the solution on the UV–Vis spectrophotometer (JASCO V – 670) till the solutions showed permanent yellow and ruby red colour respectively. TEM imaging, SAED pattern and EDAX analysis were executed using JEOL JEM 2100 high resolution transmission electron

microscope (HR-TEM) with an accelerating voltage of 200 KV. XRD patterns for the centrifuged and dried samples were recorded using X–ray BRUKER D8 Advance X-ray diffractometer with Cu Kα source (λ=1.5406 A°). FTIR spectrum was recorded using SHIMADZU, IRAffinity 1 spectrometer. A differential light scattering Malvern Zetasizer Nano ZS (Malvern Instruments Ltd., UK) instrument was used for zeta potential measurements.

2.6. Antibacterial activity

The antibacterial activity of both nanoparticles against two pathogenic microorganisms, *P.aeruginosa and S.aureus*, which were clinically isolated, was studied by zone inhibition method using sterilized Muller Hinton agar. The inoculum from the isolates was spread onto the plate using L-rod and the wells were made in the agar plate using a well borer. Colloidal silver (S_1) and gold (G_1) nanoparticles with a volume of 10 µL, 20 µL and 30 µL were added into each one of these wells. Analysis of the plates was carried out and the zones of inhibition after incubating for 24 h at 37°C in an aerobic incubation chamber.

2.7 Catalytic reduction of 4-nitrophenol and methylene blue

100 µL of 1 x 10^{-2} M 4-NP aqueous solution was added to 1.5 mL of freshly prepared 3 x 10^{-2} M $NaBH_4$ solution in a quartz cell to study the catalytic reduction activity of 4-NP. Followed by addition of 25 µL of the synthesized AgNPs (S_1 & S_5) or AuNPs (G_1 & G_5) solution to each one of these mixtures. The progress of the reaction was monitored through JASCO V–670 spectrophotometer during the conversion of 4-NP to 4-AP at room temperature between 200 and 550 nm wavelength range.

For studying the degradation process of MB, 1 mL 0.05 M $NaBH_4$ solution was added to 5 mL of 1 x 10^{-4} M Methylene blue while stirring the solution for five minutes. Then, 4 mL of Ag(S_1 & S_5) or 4 mL of Au (G_1 & G_5) colloidal solutions were added to each one of the solutions and the stirring continued for five more minutes. In the presence of $NaBH_4$ and catalyst, reduction takes place resulting in conversion of MB which was in blue colour in an oxidizing environment to colorless Leucomethylene Blue.

3. Results and discussion

3.1. Effect of concentration of metal ion solution and reaction temperature

Figure 1 depicts the UV–Vis spectra recorded during the formation of AgNPs and AuNPs from different concentrations of $AgNO_3$ and $HAuCl_4$. When the reaction went to completion, yellow and ruby-red colors were observed in silver and gold solutions respectively, representing the formation of NPs. Reddish yellow and groovy pink-ruby colours for Ag and Au NPs are known to emerge from surface plasmon vibrations [34, 35]. Extinction spectra of Ag hydrosol synthesized from different concentrations of $AgNO_3$ and $HAuCl_4$ have shown characteristic surface plasmon absorption bands at 425 nm for AgNPs and at 538 nm for AuNPs synthesized from 1.0 x 10^{-3}M of $AgNO_3$ (S_1) and $HAuCl_4$ (G_1) using a fixed volume (1 mL) of the fruit extract.

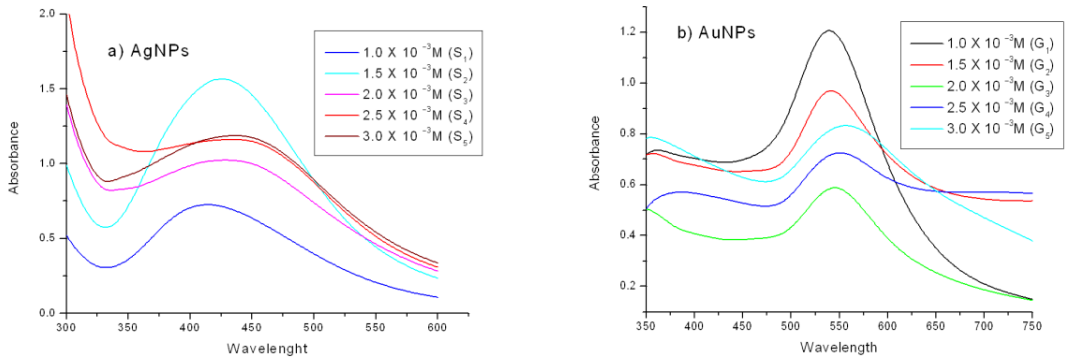

Figure 1 UV-Vis spectra of (a) AgNPs and (b) AuNPs at various concentration of $AgNO_3$ and $HAuCl_4$

The SPR band showed a shift to higher wavelength with increasing concentration of silver nitrate from 1.0 x 10^{-3}M to 3.0 x 10^{-3}M and the corresponding colour changes are observed from reddish yellow to brown; similarly the corresponding colour of the AuNPs was also observed to change from ruby-red to purple colour. The broadening as well as shift SPR band from 425 to 442 nm for AgNPs and 538 to 549 nm for AuNPs can be attributed to the increase in particle size which is also confirmed by the TEM micrographs. This kind of phenomenon has earlier been reported in the case of AgNPs synthesized using seed extract of *Jatropha curcas* [36].

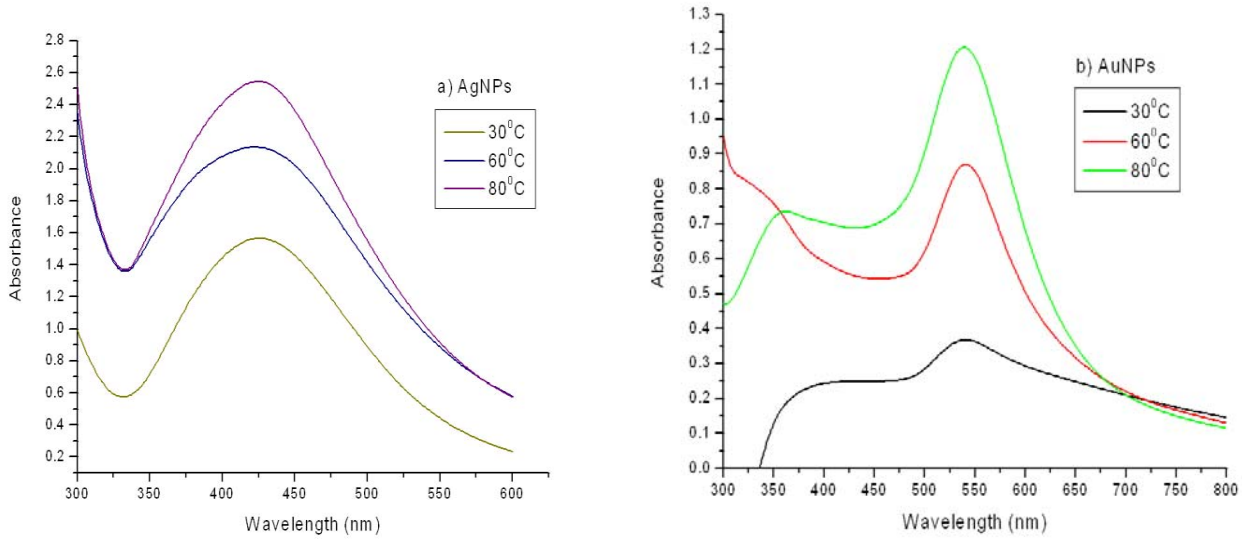

Figure 2 UV-Vis spectra of (a) AgNPs and (b) AuNPs at fixed concentration (1.0 X 10 $^{-3}$M) during the reaction at different temperatures

No shift in the wavelength of the absorption peaks was observed at fixed concentration of the metal salt solution during the reaction with extract at different temperatures (Figure 2). When the reaction was carried out at 60° and 80° C, the rate of formation of nanoparticles was observed to increase. Table 1. gives data on time and temperature dependence of nanoparticle formation during the reaction. This illustrates that SPR band at 425 nm was observed for AgNPS at 30° C after 340 min but the same band appeared within 20 min when the reaction temperature was raised to 80° C. Similarly for gold NPs, the SPR band was observed at 538 nm at 30° C in 100 min appeared within 5 min at 80° C, which also indicating that the formation of gold nanoparticles at both the temperatures was faster than silver NPs, which might be attributed to the higher reduction potential of Au^{3+} ions than Ag^{+} ions [37], similar results have been reported during the synthesis of gold nanotriangles using lemongrass extract [38].

Table 1. Effect of concentration and reaction temperature on synthesis of nanoparticles using 1 mL of fruit extract

S.No	Conc. of $AgNO_3$	Time taken for formation of AgNPS(Approx. in min)			Conc. of $HAuCl_4$	Time taken for formation of AuNPS(Approx. in min)		
		30^0C	**60^0C**	**80^0C**		**30^0C**	**60^0C**	**80^0C**
1	1.0 mM	340	35	20	1.0 mM	100	15	05
2	1.5 mM	320	30	20	1.5 mM	90	10	04
3	2.0 mM	320	28	15	2.0 mM	80	10	03
4	2.5 mM	300	21	10	2.5 mM	50	08	03
5	3.0 mM	300	20	09	3.0 mM	40	08	01

3.2. X-ray diffraction studies

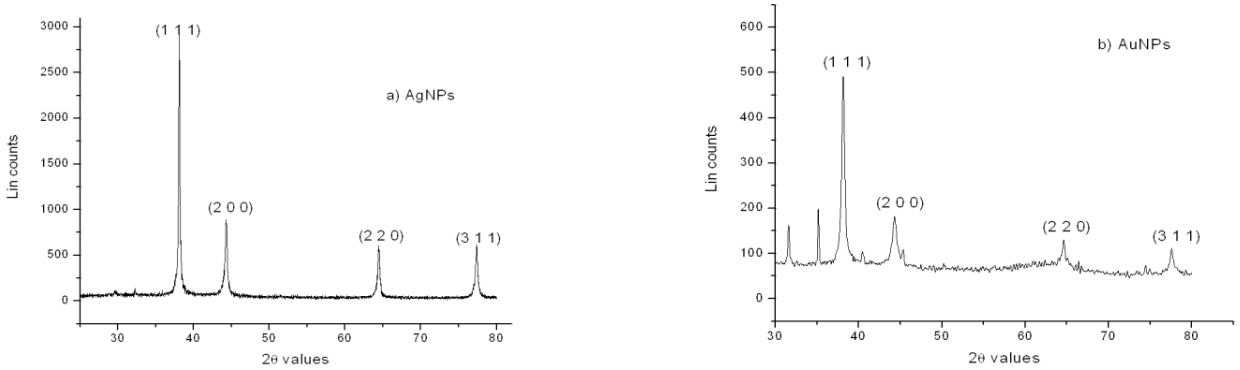

Figure 3 X-ray diffraction pattern of the dried (a) silver and (b) gold nanoparticles

The X-ray diffraction pattern (Figure 3) of the dried NPs indicates their spherical crystalline structure which is found to be polydispersed and have different particle size. Diffraction peaks (111), (200), (222) and (311) planes confirm the characteristic face-centered cubic phase (JCPDS File No.87-0720). The average size of the formed silver and gold NPs, as calculated using Debye–Scherrer equation were found to be around 35 nm and 20 nm respectively. The Bragg reflections (2 0 0), (2 2 0) and (3 1 1) were weak and broadened relative to intense (1 1 1) reflection which shows that the nanocrystals are primarily oriented along (1 1 1) plane and have small particle size as confirmed by TEM micrographs.

3.3. TEM, EDX and Zeta potential analysis

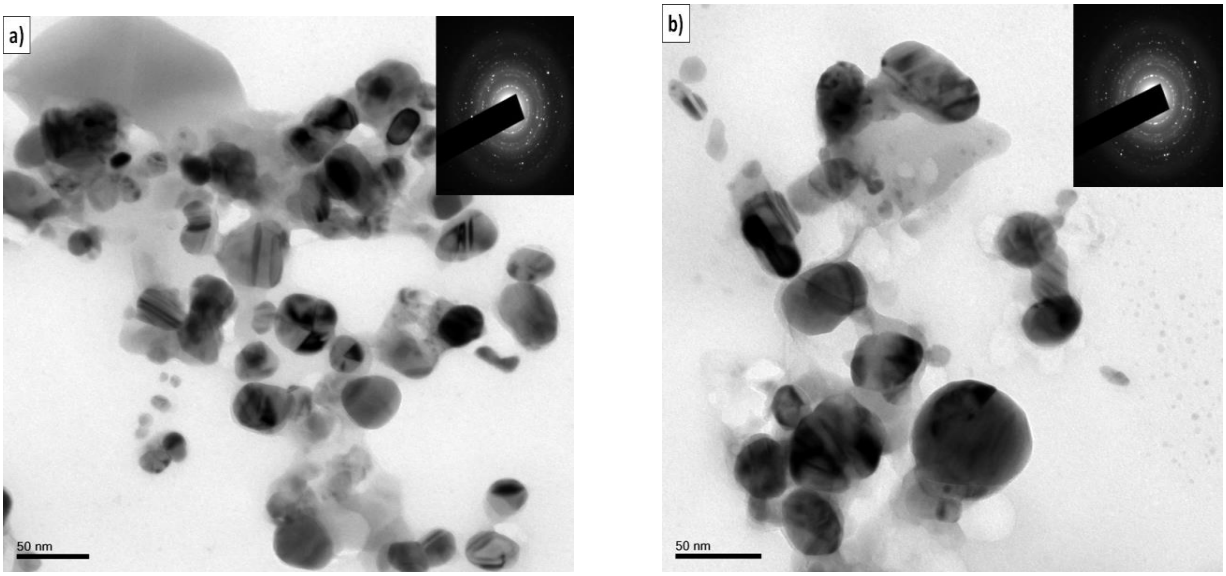

Figure 4 TEM micrograph of AgNPs synthesized from (a) 1.0 X 10^{-3}M $AgNO_3$ (S_1) and fruit extract (1 mL), (b) TEM image of larger particles synthesized from 3.0 X 10^{-3}M (S_5) $AgNO_3$ solution and fruit extract (1 mL) (inset shows the SAED pattern of nanocrystalline silver)

TEM image of AgNPs synthesized by treating 1.0 x 10^{-3}M (S_1) and 3.0 x 10^{-3}M (S_5) $AgNO_3$ solutions with 1 mL of fruit extract is shown in Figure 4 (a) & (b). These micrographs indicate that the AgNPs formed were primarily spherical with a diameters range of 25 to 40 nm and 30 to 45 nm respectively for S_1 and S_5 respectively. Particle sizes of the AgNPs synthesized using two different concentrations of $AgNO_3$ are in complete agreement with the observed SPR bands at 425 and 442 nm respectively.

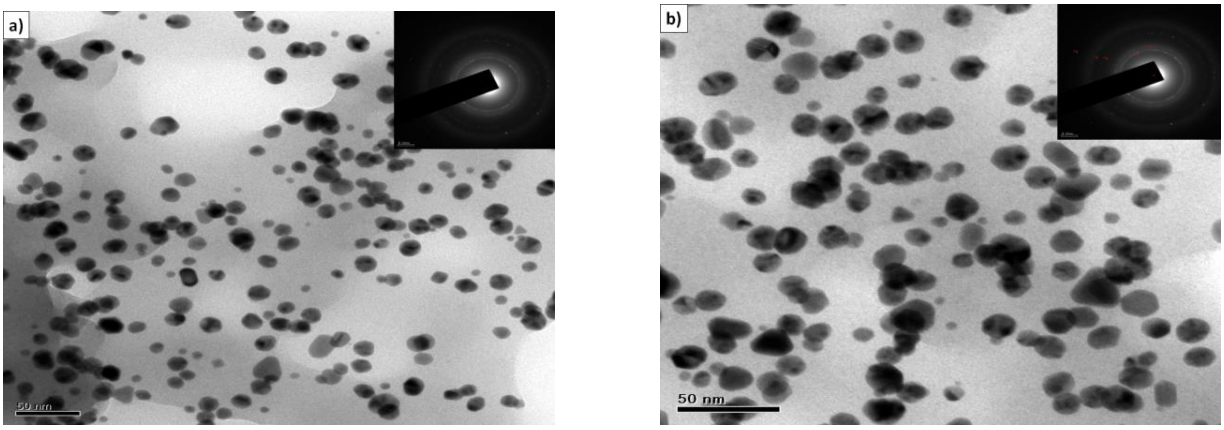

Figure 5 TEM micrograph of gold nanoparticles synthesized from (a) 1.0 X 10^{-3}M (G_1) $HAuCl_4$ and fruit extract (1 mL), (b) TEM image of larger particles synthesized from 3.0 X 10^{-3}M (G_5) $HAuCl_4$ solution and fruit extract (1 mL) (inset shows the SAED pattern of monocrystalline gold)

Similarly TEM images of AuNPs synthesized from 1.0 x 10^{-3}M (G_1) and 3.0 x 10^{-3}M (G_5) $HAuCl_4$ shown in Figure 5 (a) & (b), indicate that the average particle size has a range between 7 nm to 20 nm and 15 nm to 35 nm respectively for G_1 and G_5, which is in agreement with the observed SPR bands at 538 and 549 nm. Insets of TEM images show the selected area electron diffraction (SAED) pattern confirming the polycrystalline nature of the synthesized NPs. The TEM images taken after storing the nanoparticle solutions for 10 days showed very little agglomeration in AgNPs while no agglomeration was found in gold NPs. From this, it could be concluded that kiwi fruit extract might be acting as reducing and stabilizing agent as well. TEM images show that the small particle clusters are concealed with a thin organic layer, which acts as a capping agent since the NPs exhibits a very good distribution inside the bio-reduced aqueous phase, even in microscopic scale.

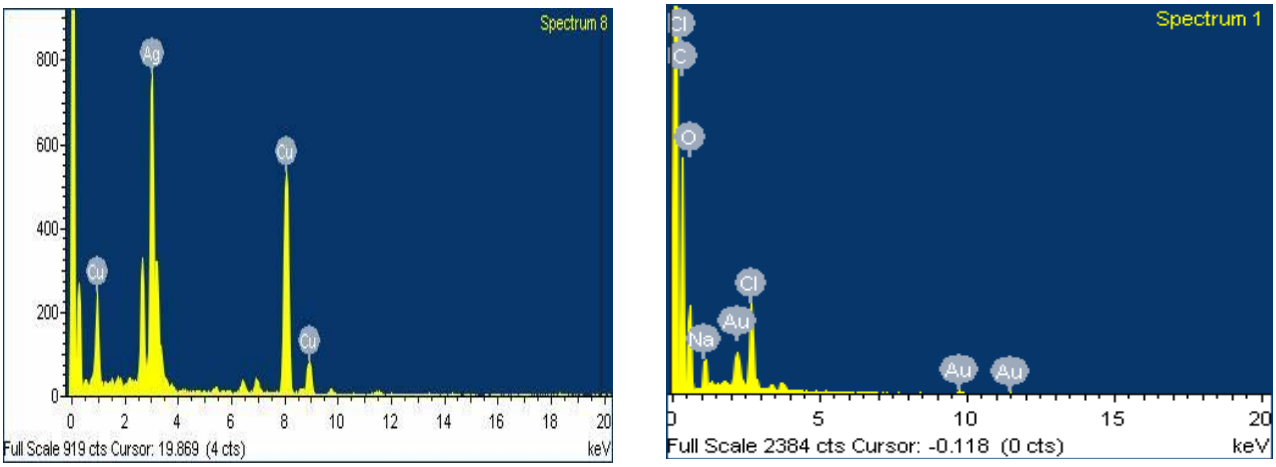

Figure 6 The optical absorption spectrum at 3 keV indicating the presence of (a) metallic Ag and absorption spectrum at 2 keV indicates the presence of (b) metallic Au

EDAX results confirmed that silver and gold are the major elements. The optical absorption spectrum at 3 keV [39] [Figure 6(a)] indicated the presence of metallic silver and the optical absorption spectrum at 2 keV [40] [Figure 6(b)] indicated the presence of metallic gold. The zeta potential values of S_1 and G_1 have been indicated as -1.46 and -22.3 mV (Figure 7). It is necessary to mention that the silver nanoparticles showed lower potential due to little agglomeration of the particles as indicated in TEM images while gold nanoparticles have shown high zeta potential value because of uniform distribution of particles.

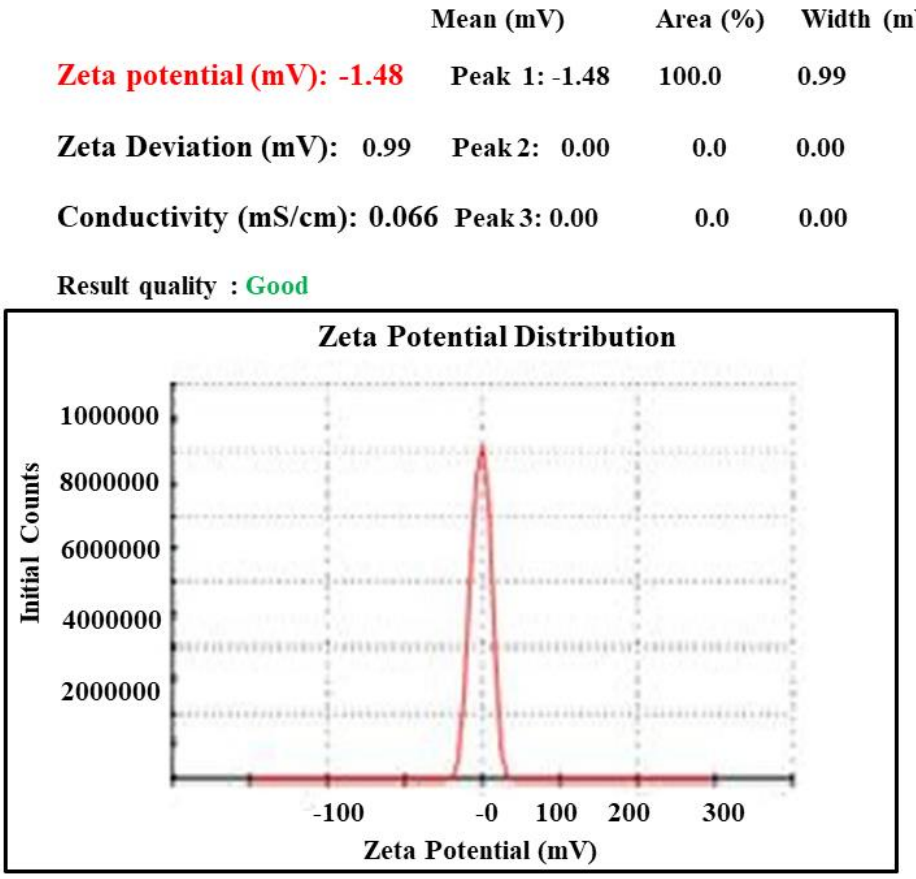

(a)

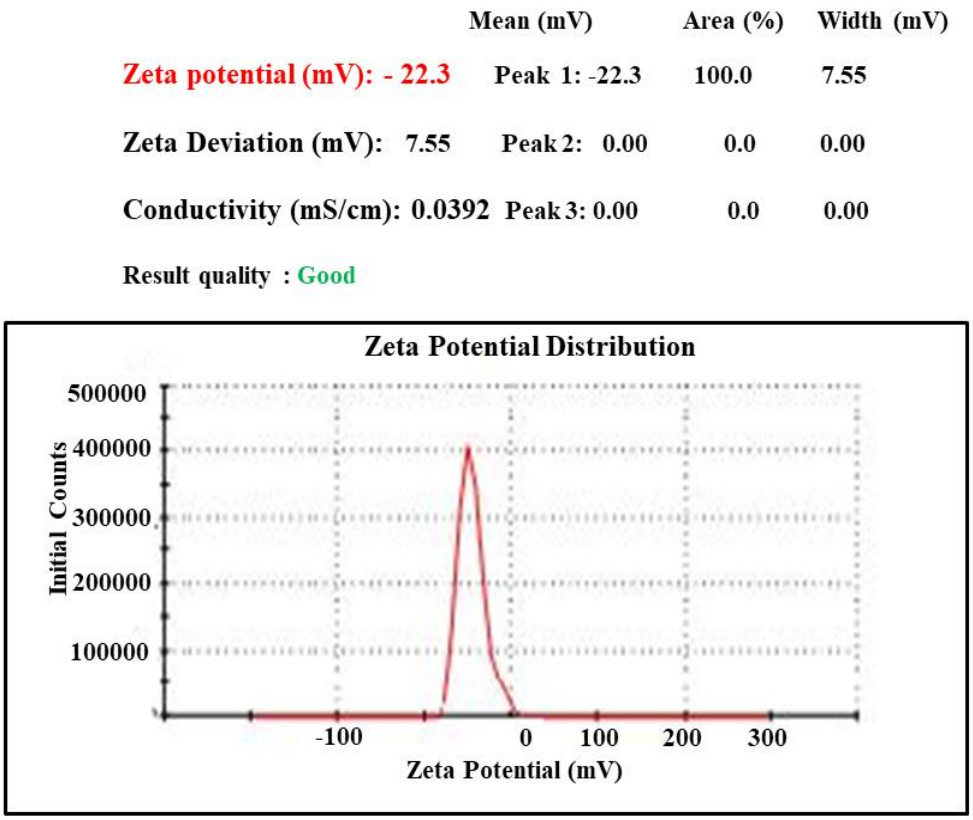

Figure 7 Zeta potential of (a) silver (S_1) and (b) gold (G_1) NPs synthesized from 1.0 X 10^{-3}M $AgNO_3$ and $HAuCl_4$ respectively

3.4. FTIR analysis

The FTIR spectra were analyzed for identification of possible functional groups which help in formation of nanoparticles. The FTIR spectrum of fruit extract (Figure 8) showed peaks at 3448 cm^{-1} corresponding to free N–H (primary amine), at 1639 cm^{-1} corresponding to – C = C – vibration, which supports the presence of some proteins. It has been reported earlier that proteins present in the kiwi fruit extract might act as a capping agents for the synthesized nanoparticles [41, 42]. Gole et al. [43] also reported that proteins are capable of capping the AuNPs by free amine groups or cysteine residues present in the proteins.

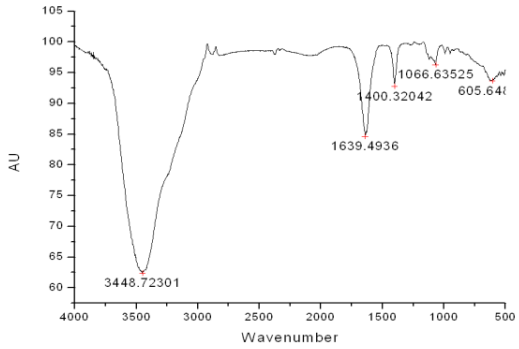

Figure 8 FTIR spectrum of Kiwi fruit extract

3.5. Antimicrobial activity of silver and gold NPs

To evaluate the antibacterial activity, the $S_1$and G_1 particles have been utilized due to their smaller particle size [44]. Two clinically isolated pathogens *P. aeruginosa* and *S. aureus* from the patient's blood have been used for the antimicrobial activity study. AgNPs showed excellent antimicrobial activity for the two replicates as presented in Figure 9 (a). The antimicrobial activity of the nanoparticles has direct correlation with increase in its concentration (Table 2) [45], which could be attributed to larger quantum of nanoparticles available to kill the microorganisms. The existence of thin peptidoglycon layer in its cell wall of Gram –ve bacterium facilitates easy penetration of silver and AuNPs making them strong antimicrobial agents against *P. aeruginosa* as seen by the maximum zone of inhibition. The smaller zone of inhibition noticed for Gram +ve bacteria may be because of the strong structure of linear polysaccharide making penetration of nanoparticles difficult [46]. The significant bactericidal activity observed may be due to the released silver cations which change the membrane characteristics resulting in increased membrane permeability of the bacteria [47, 48]. Several reports indicate death of bacteria by rupturing of cell wall and denaturation of protein when the silver ions of AgNPs gets attached to the negatively charged cell wall of bacteria [49]. Accumulation of envelope protein precursors takes place when the cell wall of bacteria gets explicitly attached to silver ions or nanoparticles. Interestingly, Lok et al. [50] have brought out that depletion of intercellular ATP occurs due to the destabilization of outer membrane and rupture of the plasma membrane when interacted by silver NPs. Sarkar et al. [51] have also reported that compared to penicillin, AgNPs showed greater bactericidal efficiency against *S. aureus*. The AuNPs synthesized showed excellent inhibition zone [Figure 9(b)] against all the test organisms but the activity was observed to be less compared to AgNPs. Furthermore, the nanoparticles synthesized by green route were found to be highly operative against Gram -ve bacteria, though the exact mechanism is not yet known.

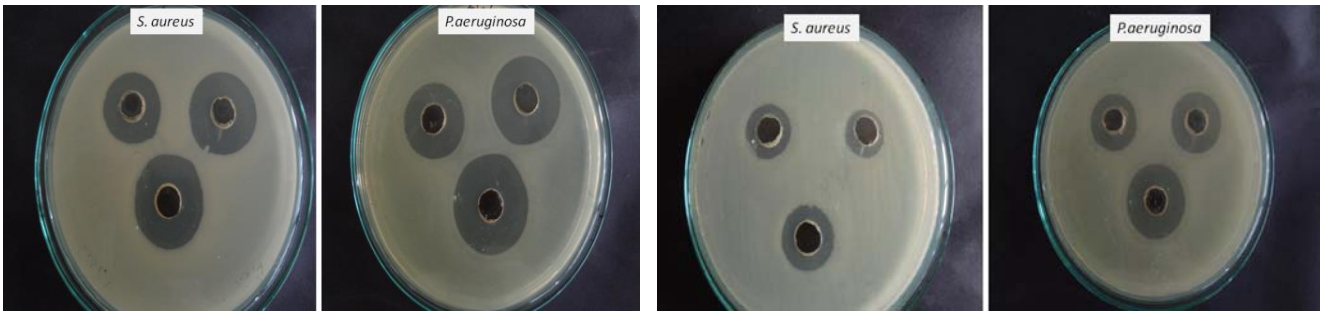

Figure 9 (a) Antibacterial activity of AgNPs synthesized from 1.0 X 10^{-3}M $AgNO_3$ (S_1) (b) activity of AuNPs synthesized from 1.0 X 10^{-3}M $HAuCl_4$ (G_1).

Name of the pathogen	Zone of inhibition for AgNPs (in mm)			Zone of inhibition for AuNPs (in mm)		
	10 µL	**20 µL**	**30 µL**	**10 µL**	**20 µL**	**30 µL**
P.aeruginosa	20	25	27	15	16	21
S.aureus	18	20	20	12	17	20

Table 2. Bactericidal activity of silver and AuNPs synthesized from 1.0 x 10^{-3}M $AgNO_3$ (S_1) and $HAuCl_4$ (G_1) respectively

3.6. Catalytic degradation of 4-nitrophenol

The catalytic reduction of 4-NP in the presence of AgNPs (S_1 & S_5) and AuNPs (G_1 & G_5) was checked by UV-Vis spectroscopy. Reduction of 4-NP to 4-AP by aqueous $NaBH_4$, though thermodynamically favored, the kinetic barrier decreases the feasibility of the reaction due to large potential difference between donor and acceptor molecules. The metal NPs catalyze this reaction by promoting electron relay from the donor BH^{4-} to acceptor 4-NP to overcome the kinetic barrier. The 4-NP shows a red shift in an absorbance peak from 317 nm to 400 nm due to the formation of 4-nitrophenolate ion in the alkaline medium caused by $NaBH_4$ [52]. The data in Figure 10(a) indicates that the reduction gets completed in 33 min in the presence of S_5 nanoparticles, with the yellow colour of 4-NP disappearint. However, the reaction in the presence of S_1 nanoparticles [Figure10 (b)] takes only 22 min for completion. Similarly the reduction of 4-NP in the presence of G_5 nanoparticles [Figure 10 (c)] gets completed in 20 min while with G_1 nanoparticles [Figure 10 (d)] it takes 14 min for completion . The reaction was carried out with water as control in place of nanoparticle solution and the peak at 400 nm remained unchanged even after 5 days, thus the catalytic role of nanoparticles in the reduction process. Plots of ln (A) vs time for the reduction of 4-NP by $NaBH_4$ in the presence of both metal nanoparticles shown in Fig. 12 (a) & (b) are linear through 90% completion of the reaction. Decrease in reaction rate was observed with the increase in concentration of metal ion solution. Such decrease in catalytic activity with increase in metal ion concentration could be because of increase in particle size, as seen in TEM and DLS measurements. Esumi et al. [53] have reported similar trend in the catalytic activity of dendrimer metal nanocomposites during the reduction of 4-NP with increase in the concentration of dendrimer.

.

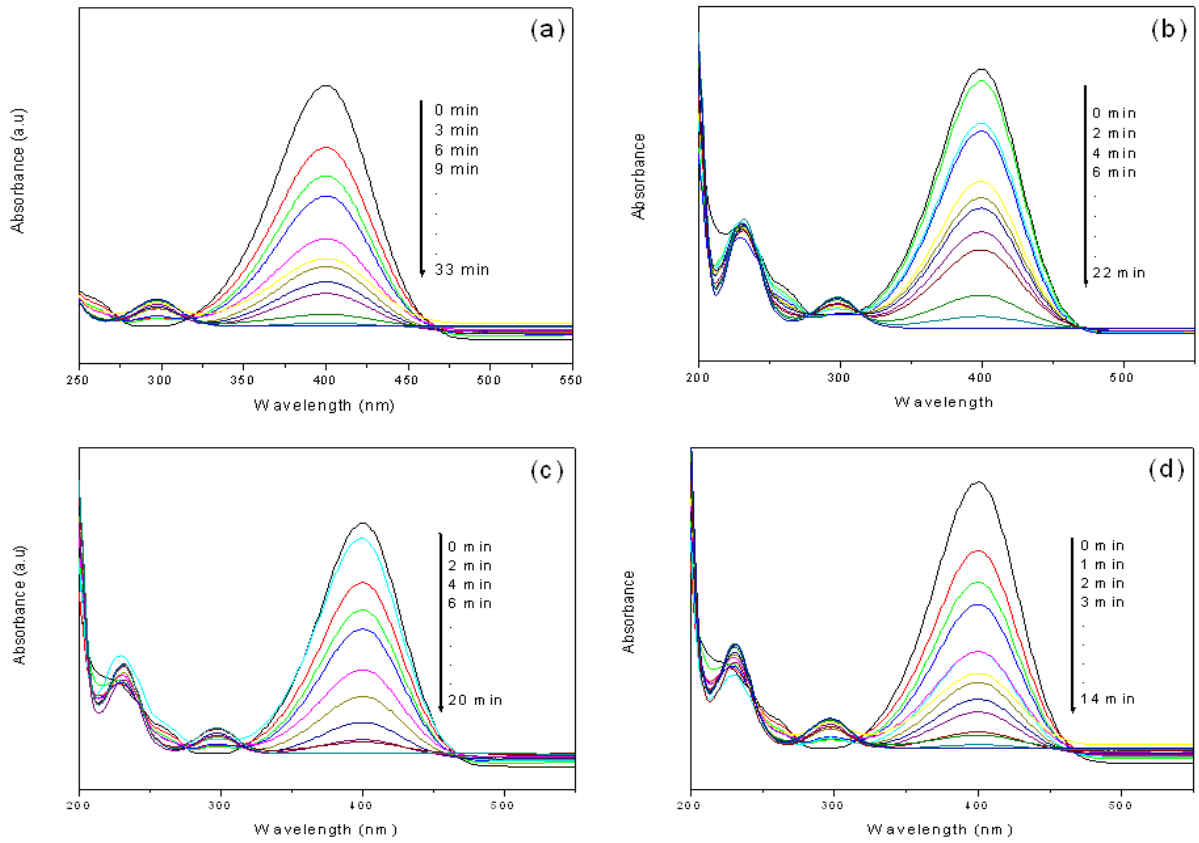

Figure 10 Time-dependent UV-Visible spectra for the catalytic reduction of 4-NP by NaBH4 in the presence of (a) S5 (b) S1 (c) G5 and (d) G1 catalysts obtained from 1 mL of extract

3.7. Catalytic degradation methylene blue

Kinetics of catalytic reduction of MB has been studied in the presence of $NaBH_4$. The rate of reduction of MB is evaluated by plotting relative absorbance at 664 nm and 614 nm as a function of time. The main absorption band at 664 nm is reported to correspond to n-π* transition of MB. During reduction reaction of MB it converts to its reduced form Leuco MB (LMB) [54, 55]. Figure 11 (a) shows the reduction of MB in the presence of S_5 catalyst over a time period of 39 min, the observed decrease in absorbance indicating that the reduction of MB is a slow process. The reduction is found to get accelerated in the presence of S_1 catalyst [Figure 11 (b)] and goes to completion in 24 min which is indicated by a strong decrease in the absorbance. Similarly particle size dependence on rate of catalytic reduction of MB to LMB was also investigated in the presence of G_5 and G_1 catalysts. From Figure 11 (c), it can be seen that the time required for complete reduction of MB is recorded as 33 min in the presence of G_5 catalyst, while G_1 catalyst [Figure 11 (d)] helped completion of the reduction in 21 min. Figure 12 (c) & (d) shows linear relation of ln (A) vs time for the reduction of MB to LMB in the presence of both metal nanoparticles till 90% completion of the reaction. The increase in reaction time with the increase in metal ion concentration might be because of increase in size of the particles as explained earlier in 4-NP reduction. The redox potential of AgNPs shoud be located between the redox potential of donor ($NaBH_4$) and acceptor (MB) system for efficient catalysis [56]. Due to electron relay effect, the metal nanoparticles act as electron transfer mediators between MB and $NaBH_4$ during their action as a redox catalyst.

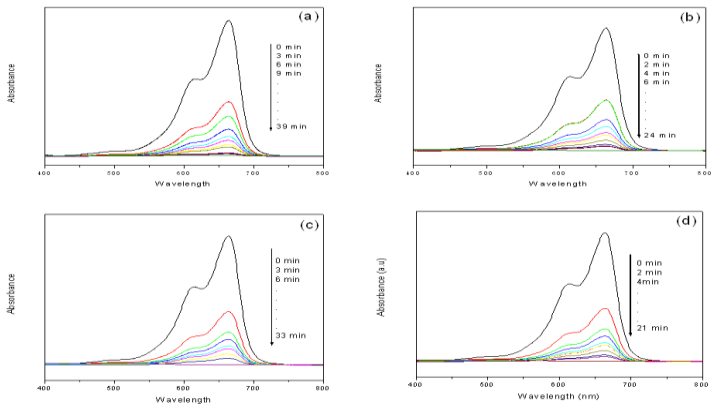

Figure 11 Time-dependent UV-Visible spectra for the catalytic reduction of MB by $NaBH_4$ in the presence of (a) S_5 (b) S_1 (c) G_5 t and (d) G_1 catalyst obtained from 1 mL of extract

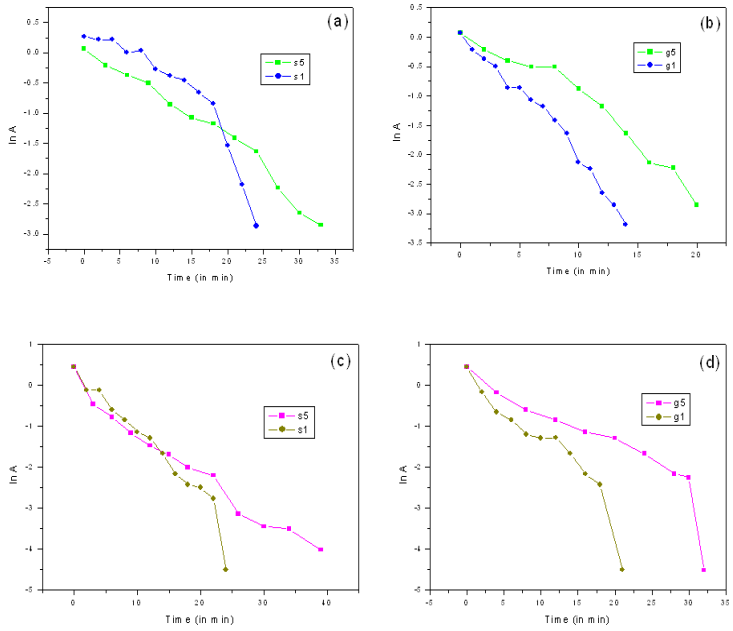

Figure 12 Comparative plots of ln (A) vs t for (a) S_5 & S_1 (b) G_5 & G_1 towards the reduction of 4-NP. Comparative plots of ln (A) vs t for (c) S_5 & S_1 (d) G_5 & G_1 towards the reduction of MB in the presence of $NaBH_4$

4. Conclusion

Silver and AuNPs have been successfully synthesized using kiwi fruit extract, an environmentally benign and renewable fruit which acts as reducing as well as stabilizing agent. UV-Vis spectroscopy and TEM micrographs of the synthesized silver and gold hydrosol suggest that with the increase of concentration of aqueous solutions, the particle size increases due to which broadening and shifting of SPR band takes place. The adopted method requires only a few minutes to achieve higher than 90% conversion when the reaction temperature was raised to 80° C. The synthesized NPS have exhibited good catalytic activity during the reduction of two organic pollutants 4-NP and MB. With the decrease in size of the nanoparticles, the reaction time is observed to decrease due to their higher surface area. In addition, the synthesized nanoparticles have also exhibited excellent antibacterial activity against clinically isolated *P.aeruginosa* and *S.aureus.*

Acknowledgements

The help extended by Dr Balachandran Unni Nair, Chief Scientist and Head, Chemical Laboratory, Central Leather Research Institute, CSIR Chennai, India for carrying out zeta potential measurements using Malvern Zetasizer Nano ZS instrument is gratefully acknowledged. The authors also thank the help extended by VIT University, Vellore, India.

References

[1] Smith AM, Duan H, Rhyner MN, Ruan G, Nie S 2006 *Phys Chem Ch Ph*. **33** 3895–3903
[2] Hernández-Sierra JF, Ruiz F, Pena D, Martinez-Gutierrez F, Martinez AE, Guillén AJP, Tapia-Pérez H, Castañón GM 2008 *Nanomedicine* **4** 237–240
[3] Dror-Ehre A, Mamane H, Belenkova T, Markovich G, Adin A 2009 *J Colloid Interface Sci* **339** 521–526
[4] Eby DM, Schaeublin NM, Farrington KE, Hussain SM, Johnson GR 2009 *ACS Nano* **3** 984–994
[5] Panacek A, Kola M, Vecerova R, Prucek R, Soukupova J, Krys tof V, Hamal P, Zboril R, Kvı tek L 2009 Biomaterials **30** 6333–6340
[6] Fayaz AM, Balaji K, Girilal M, Yadav R, Kalaichelvan PT, Venketesan R 2010 *Nanomedicine* **6** 103–109
[7] Da-Guang Y 2007 *Colloids Surf B* **59** 171-178
[8] Liu YC and Lin LH 2004 *Electrochem Commun* **6** 1163–1168
[9] Mallick K, Witcombb MJ, Scurrella MS 2005 *Mater Chem Phys* **90** 221–224
[10] Bae CH, Nam SH, Park SM 2002 *Appl Surf Sci* **197** 628–634
[11] Anstas PT, Warner JC 1998 Green Chemistry: Theory and Practice, New York Oxford University Press Inc.
[12] De Simone JM 2002 *Science* **297** 799–803
[13] Gross RA and Kalra B 2002 Science **297** 803–807
[14] Poliakoff M and Anasta P 2001 *Nature* **413** 257–265
[15] Raveendran P, Fu J, Wallen SL 2003 *J Am Chem Soc* **125** 13940–13941
[16] Zhang WB, Xiao XM, An TC, Song ZG, Fu JM, Sheng GY, Cui MC 2003 *J Chem Technol Biotechnol* **78** 788–794
[17] Oturan MA, Peiroten J, Chartrin P, Acher AJ 2000 *Environ Sci Technol* **34** 3474–3479

[18] Akpan UG and Hameed BH 2009 *J Hazard Mater* **170** 520–529

[19] Díaz-Cruz MS and Barceló D 2008 *Chemosphere* **72** 333–342
[20] Small JM and Hintelmann H 2007 *Anal Bioanal Chem* **387** 2881–2886
[21] Burhenne J, Riedel KD, Rengelshausen J, Meissner P, Müller O, Mikus G, Haefeli WE, Walter-Sack I 2008 *J Chromatogr B* **863** 273–282
[22] Sahoo NK, Pakshirajan K, Ghosh PK 2011 *J Hazard Mater* **190** 729–737
[23] Arora PK and Jain RK 2012 *PLoS One* **7** e38676.
[24] Narayanan KB, Park HH, Sakthivel N 2013 *Spectrochim Acta A* **116** 485–490
[25] Vidhu VK, Philip D 2014 *Spectrochim Acta A* **117** 102–108
[26] Saraschandra Naraginti and Sivakumar A 2014 *Spectrochim Acta A* **128** 357–362
[27] Yudha SS, Notriawan D, Angasa E, Suharto TE, Hendri J, Nishina Y 2013 *Mater Lett* **97** 181–183
[28] Prathna TC, Chandrasekaran N, Raichur MA, Mukherjee A. 2011 *Colloids Surf B* **82** 152–159
[29] Philip D 2010 *Physica E* **42** 1417–1427
[30] Noruzi M, Zare D, Khoshnevisan K, Davoodi D 2011 *Spectrochim Acta A* **79** 1461–1465
[31] Prabha Dubey S, Lahtinen M, Sillanpaa M 2010 *Colloids Surface A* **364** 34–41
[32] Ganesh Kumar V, Dinesh Gokavarapu S, Rajeswari A, Stalin Dhas T, Karthick V, Kapadia Z, Shrestha T, Barathy IA, Roy A, Sinha S 2011 *Colloids Surf B* **87** 159–163
[33] Lee HJ, Song JY, Kim BS 2013 *J Chem Technol Biotechnol* **88** 1971–1977
[34] Tripathi A, Chandrasekaran N, Raichur AM, Mukherjee A 2009 *J Biomed Nanotechnol* **5** 93–98
[35] Vivekanandhan S, Misra M, Mohanty AK 2009 *J Nanosci Nanotechnol* **9** 6828–6833
[36] Bar H, Bhui DK, Sahoo GP, Sarkar P, Pyne S, Misra A 2009 *Colloids Surf A* **348** 212–216
[37] Song JY, Kim BS 2009 *Bioprocess Biosyst Eng* **32** 79–84
[38] Rai A, Singh A, Ahmad A, Sastry M 2006 *Langmuir* **22** 36–741
[39] Magudapathy P, Gangopadhyay P, Panigrahi B K, Nair KGM, Dhara S 2001 *Physica B* **299** 142–146
[40] Alvarez MM, Khoury JT, Schaaff TG, Shafigullin MN, Vezmar I, Whetten RL 1997 *J Phys Chem B* **101** 3706–3712
[41] Li S, Shen Y, Xie A, Yu X, Qiu L, Zhang L, Zhang Q 2007 *Green Chem* **9** 852–858
[42] Shankar SS, Ahmad A, Sastry M 2003 *Biotechnol Progr* **19** 1627–1631
[43] Gole A, Dash C, Vidya R, Sainkar SR, Mandale AB, Rao M, Sastry M 2001 *Langmuir* **17** 1674–1679
[44] Lu Z, Rong K, Li J, Yang H, Chen R 2013 *J Mater Sci Mater Med* **24** 1465–1471
[45] Kim JS, Kuk E, Yu KN, Kim JH, Park SJ, Lee HJ, Kim SH, Park YK, Park YH, Hwang CY, Kim YK, Lee YS, Jeong DH, Cho MH 2007 *Nanomedicine* **3** 95–101
[46] Shrivastava S, Bera T, Roy A, Singh G, Ramachandrarao P, Dash D 2007 *Nanotechnology* **18** 225103-225111
[47] Dibrov P, Dzioba J, Gosink KK, Hase CC 2002 *Antimicrob Agents Chemother* **46** 2668–2670
[48] Sondi I, Sondi BS 2004 *J Colloid Interface Sci* **275** 177–182
[49] Lin YE, Vidic RD, Stout JE, McCartney CA, Yu CL 1998 *Water Res* **32** 1997–2000
[50] Lok CN, Ho CM, Chen R, He QY, Yu WY, Sun H, Tam PK, Chiu JF, Che CM 2006 *J Proteome Res* **5** 916–924
[51] Sarkar S, Jana AD, Samanta SK, Mostafa G 2007 Polyhedron **26** 4419–4426
[52] Pradhan N, Pal A, Pal T 2002 *Colloids Surf A* **196** 247–257
[53] Esumi K, Isono R, Yoshimura T 2004 *Langmuir* **20** 237–243
[54] Rauf MA, Meetani MA, Khaleel A, Ahmed A 2010 *Chem Eng J* **157** 373–378

[55] Laoufi I, Lazzari R, Jupille J, Robach O, Garaud S, Cabaih G, Dolle P, Crugel H, Baillly AJ 2001 *J Phys Chem C* **115** 4673–4679

[56] Jana NR, Sau TK, Pal T 1999 *J Phys Chem B* **103** 115–121